Test Methodology for Automotive Surround Sensors in Dynamic Driving Situations

Alexander Kamann*, Sinan Hasirlioglu*, Igor Doric*, Thomas Speth*, Thomas Brandmeier* and Ulrich T. Schwarz†
*Center of Automotive Research on Integrated Safety Systems and Measurement Area (CARISSMA)
Technische Hochschule Ingolstadt, 85049 Ingolstadt, Germany
Email: {alexander.kamann, sinan.hasirlioglu, igor.doric, thomas.speth, thomas.brandmeier}@thi.de
†Experimental Sensor Science, Chemnitz University of Technology, 09126 Chemnitz, Germany
Email: ulrich.schwarz@physik.tu-chemnitz.de

***Abstract*—Modern vehicles use surround sensors to measure their local environment. The information are processed and forwarded to intelligent pre-crash or automation functions enhancing vehicle safety or enabling automated driving. False or inaccurate measurements can lead to fatal consequences for humans and vehicles. High accuracy and robust environment perception in all driving situations, including high dynamic driving situations e.g. skidding, are compulsory requirements for these systems. Therefore, automotive surround sensors must be tested in various driving situations. This paper presents a new, non-destructive and reproducible test methodology for testing surround sensors in high dynamic driving situations. Therefore, the vehicle's motion during a skid driving situation was mathematically described. The test methodology was validated through experiments carried out with a real test vehicle. Finally, the experimental setup and the results are presented and discussed.**

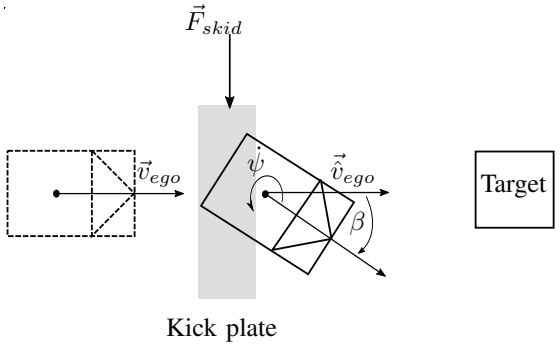

Fig. 1. Principle of the test methodology applying an additional force to transfer the vehicle in a high dynamic driving situation

I. Introduction

On average, more than two persons are killed every minute in road traffic and up to hundreds are injured worldwide. In absence of measures, traffic accidents will be the seventh leading cause of death by 2030 [1]. To overcome this problem, the development of novel automotive safety systems is mandatory. Safety systems like airbags and seat belts have become essential safety devices by providing cushioning and restraint during a crash event. Irreversible restraint systems aim to prevent forces between occupants and interior of the vehicle [2]. Collision avoidance or mitigation systems can be realized by using pre-processed information of surround sensors e.g. radar sensors. Collision mitigation systems aim to warn the driver before a collision is going to occur, using acoustic signals. Subsequently, the system can reduce the crash severity autonomously by braking or steering if the collision is unavoidable. Pre-crash systems based on radar sensors can be found in [3] and [4]. If the system determines an imminent and unavoidable collision before there is a mechanical contact, enhanced airbag systems can be employed e.g. for adjusting the drivers position to reduce injury severity. Pre-triggered airbags can be designed larger in volume with more extension in the vehicle's longitudinal direction. Hence, lower loads, earlier coupling of the passenger and slower inflation of the airbag can be reached and result in a less aggressive system [5]. Passive safety systems remain essential, since severe accidents are likely to occur also in future. Misfiring a pre-triggered airbag in a harmless situation can lead to severe injury or death of the passenger. Therefore, high reliability and robustness of the systems are mandatory. Hence, it is necessary to test automotive surround sensors in various specific situations e.g. under environmental influences or high dynamic driving situations. Reproducible tests decrease the test effort and support test driven development of new safety algorithms. The authors presented in [6] a methodology to observe the influence of rain on the performance of surround sensors. Water covered roads are associated with a reduced friction coefficient. This can result in a skid driving situation. Furthermore, a skid driving situation was ranked 7 of 10 main causes for traffic accidents according to ADAC crash research in 2011 [7]. This paper presents a new test methodology for the test of automotive surround sensors during high dynamic driving situations in real-world scenarios.

This paper is organized as follows: Section II introduces the test methodology for automotive surround sensors and describes a vehicle motion model in skid situations. Section III presents the experiment and measurement setup. Section IV discusses the measurement results and shows the effects of high dynamic driving situations in comparison to regular driving situations for an automotive radar sensor. Section V summarizes the results and scientific contribution of this paper.

978-1-5090-5932-4/17/$31.00 ©2017 IEEE

II. Methodology

The presented test methodology enables non-destructive and reproducible tests of automotive surround sensors during skid events in real world scenarios.

A. Test Methodology

The presented test methodology is based on a kick plate, which applies a lateral force to the rear axle of a test vehicle, as shown in Fig. 1. The test vehicle approaches a target object, which is detected by surround sensors. The kick plate is located between vehicle and target object. At a certain time t_k, where the test vehicle approaches the target object at a specific velocity, an external force $\vec{F}_{skid}$ is applied on the rear axle by the kick plate. This force causes a rotational component to the translational motion, which affects the vehicle's yaw rate. This results in a skid driving situation under deterministic conditions. The yaw rate depends on the magnitude of external force $\vec{F}_{skid}$ and leads to a side slip angle β, which changes the direction of the longitudinal vehicle axis relative to the direction of movement. Degradation of confidence and limits of the sensor's performance, based on the used dynamic driving model, can be detected and measured in a controlled manner by incrementing the shift intensity of the kick plate. The sensor limit is reached when the distinction between real objects and false positive objects is unfeasible, e.g. two objects are close to each other during a skid event. Furthermore, the detection, classification and tracking performance for different surround sensors or safety systems can be tested by variation of reference target's position or the applied external force in different experimental setups. The following subsection describes the effect of an external lateral force $\vec{F}_{skid}$ to the vehicle dynamics using the single track model.

B. Theoretical Model

For describing the vehicle motion, pitch and roll rate are neglected. The acceleration a in the vehicle's center of mass (CoM) is given by

$$a = \dot{v} + \omega \times v = \begin{bmatrix} -v \cdot sin(\beta)\dot{\beta} \\ v \cdot cos(\beta)\dot{\beta} \\ 0 \end{bmatrix} + \begin{bmatrix} 0 \\ 0 \\ \dot{\psi} \end{bmatrix} \times \begin{bmatrix} v \cdot cos(\beta) \\ v \cdot sin(\beta) \\ 0 \end{bmatrix} = \begin{bmatrix} -v(\dot{\psi}+\dot{\beta})sin(\beta) \\ v(\dot{\psi}+\dot{\beta})cos(\beta) \\ 0 \end{bmatrix} \quad (1)$$

where β is the angle between vehicle longitudinal direction and velocity vector v of CoM, $\dot{\psi}$ the yaw rate and ω is the angular velocity.

Compared to the original single track model [8] an additional force $\vec{F}_{skid}$ is applied by the kick plate. This force is similar to side wind effects as shown in [9]. The skid event causes high magnitudes of slip angles α_f and α_r at front and rear axle and side slip angle β, thus small angle approximation could not be used. Fig. 2 shows the geometry of the used single track model. The equilibrium of forces and moments in vehicle lateral direction considering the kick plate force are as follows:

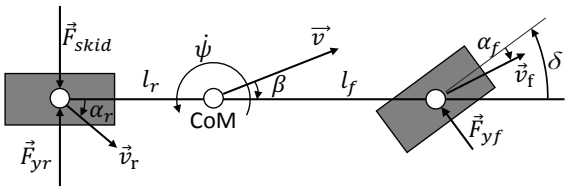

Fig. 2. Geometry of single track model considering external force by the kick plate

$$\ddot{\psi}\theta = F_{yf}cos(\delta)l_f - F_{yr}l_r + F_{skid}l_r \quad (2)$$

$$ma_y = mv(\dot{\psi}+\dot{\beta})cos(\beta) = F_{yf}cos(\delta) + F_{yr} - F_{skid} \quad (3)$$

where δ represents the steering angle of the front wheels and θ the moment of inertia. The mass m of the vehicle is centered in the CoM, which has a horizontal distance of l_r from rear axle and l_f from front axle. The lateral tire forces are defined by the product of slip angle $\alpha_{f/r}$ and corner stiffness $c_{f/r}$ in linear range.

$$F_{y,f/r} = \alpha_{f/r} \cdot c_{f/r} \quad (4)$$

The slip angles $\alpha_{f/r}$ are defined by the tires' velocity vector $v_{f/r}$. The longitudinal velocities must be equal, since the vehicle is not stretched in longitudinal direction. The difference of lateral velocities is caused by the yaw rate $\dot{\psi}$. Thus, the slip angles $\alpha_{f/r}$ are defined as follows [10]:

$$\alpha_f = -\arctan\left(\frac{v\sin(\beta) + l_f\dot{\psi}}{v\cos(\beta)}\right) + \delta \quad (5)$$

$$\alpha_r = -\arctan\left(\frac{v\sin(\beta) - l_r\dot{\psi}}{v\cos(\beta)}\right) \quad (6)$$

With equations (4) - (6) inserted in equation (2) and (3), a non-linear model describing the vehicle horizontal motion is derived of following two differential equations:

$$\ddot{\psi} = \theta^{-1}\left\{ c_f\left[-\arctan\left(\frac{v\sin(\beta) + l_f\dot{\psi}}{v\cos(\beta)}\right) + \delta\right]\cos(\delta)l_f - c_r\left[-\arctan\left(\frac{v\sin(\beta) - l_r\dot{\psi}}{v\cos(\beta)}\right)\right]l_r + F_{skid}l_r\right\} \quad (7)$$

$$\dot{\beta} = \frac{1}{mv\cos\beta}\left\{ c_f\left[-\arctan\left(\frac{v\sin(\beta) + l_f\dot{\psi}}{v\cos(\beta)}\right) + \delta\right]\cos(\delta) + c_r\left[-\arctan\left(\frac{v\sin(\beta) - l_r\dot{\psi}}{v\cos(\beta)}\right)\right] - F_{skid}\right\} - \dot{\psi} \quad (8)$$

Steering angle δ and skidding force F_{skid} are inputs of the model. The corner stiffnesses $c_{f/r}$ can not be assumed linear, as shown in Fig. 3. Lateral tire force is not proportional to slip angle, because lateral acceleration a_y is limited to approximately 1 g at good conditions and less if the road is

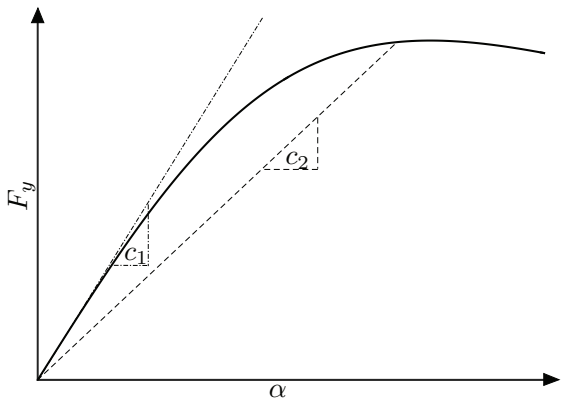

Fig. 3. Linear (c_1) and non-linear (c_2) lateral tire force characteristics

humid or dirty. Therefore, the following Magic Formula [11], [12] is used for modeling the road-tire-contact.

$$F_y = D\sin\{C\arctan[B\alpha - E(B\alpha - \arctan(B\alpha))]\} \quad (9)$$

The parameter B, C, D and E represent empirical values. The shape factor C scales the curve in x-direction. By D, the peak value is defined and with curvature factor E the curve can be additionally stretched or compressed. The product of BCD is equivalent to corner stiffness at zero slip, i.e. c_1 in Fig. 3. The slip angle is input and an adaptive corner stiffness is output of this model.

III. Experimental setup

A. Test Vehicle

A test vehicle was used to record sensor data in regular and high dynamic driving tests (e.g. skid situations). The test vehicle is equipped with an automotive radar, camera and an inertial measurement unit with six degrees of freedom. The sensors are connected to a measurement computer, which is used to record the pre-processed sensor data. Therefore, data are object-specific and provide information about objects in the sensor's field of view e.g. lateral distance to the longitudinal axis of the vehicle. The radar sensor detects objects e.g. vehicles or vulnerable road users and determines features of surrounding objects. These object information are used by automation, comfort or safety functions.
The measurements were carried out with the standardized Euro NCAP Vehicle Target (EVT) as realistic radar target. This target is used to test and validate various safety functions, e.g. emergency brake assist. Details of the target vehicle can be found in [13].

B. Regular Driving Situation

Sensor data recorded in regular driving situations without applying an external force are used to study regular sensor performance. The experimental setup for regular driving scenarios, using the reference target, was built at an outdoor test track. Therefore, the test vehicle approaches the EVT straight at a velocity of 30…55 km/h. The distance between test vehicle and EVT was set to 50 m.

TABLE I
Kick plate Parameter

Parameter	Value	Unit
Length of sliding area	10	[m]
Length of intervention area	60	[m]
Operation velocity range	30…55	[km/h]
Friction sliding area	0.2	-
Friction intervention area	0.25	-
Intensity lateral shift	1, 2, 3	-
Watered	Yes	-

C. High Dynamic Driving Situation

Kick plates are mainly used to train regular drivers stabilize the vehicle in unexpected skid situations [14]. The test runs were carried out on a kick plate test area in front of low friction areas to cause the vehicle to skid out of control. First, the vehicle is accelerated to a certain velocity, passes the kick plate, receives a lateral acceleration, slides across the low friction area and is stabilized by a test driver via steering and braking. Fig. 4 shows the acceleration path, kick plate, watered metal sliding and intervention area. Table I shows the kick plate parameters. The friction of the sliding and intervention area are under watered conditions at $\mu_{slide} = 0.2$ and $\mu_{int} = 0.25$. The vehicle's CoM can be assumed of moving straight ahead due to the low friction of the sliding area. During the sliding event the vehicle's side slip angle is increasing depending on the skid force $\vec{F}_{skid}$ of the kick plate as described in equation 8. During the sliding event the test driver did not intervene in the vehicle's driving dynamics by steering or braking. The test driver starts to stabilize the vehicle when the front axle enters the intervention area. The driving situation is divided in 3 phases, which correspond to results in Fig. 5 and Fig. 7:

- Phase I: The test vehicle is accelerated to a certain velocity. The radar beam illuminates the reference target with increasing overlap due to the vehicle trajectory on the left-curved acceleration area.
- Phase II: The kick plate is activated. The test driver does not intervene in vehicle's motion.
- Phase III: The test driver starts to stabilize the vehicle and approaches the reference target.

Several high dynamic driving situation videos can be found at **https://goo.gl/ELebkU**.

D. Radar Sensor

Radar sensors are used to percept objects in their local environment. A target is tracked using a Kalman filter after it has been detected. The probability of existence (PoE) is a feature of an object, determined by an observer. Its value increases by the number of assigned detections and accuracy within the filter calculations of the particular object. Reliable object tracking is key to enable perception of complex multiple-target situations [15]. Nowadays, vehicle field experiments are

Fig. 4. Kick plate test track with acceleration path and intervention area (top picture) and sample test run with skidding test vehicle approaching the EVT (bottom picture)

used to test automotive sensors and systems under realistic conditions [16]. These tests are necessary, but can not be used to cover the required large number of test cases and kilometers for complex functions. In [17] a method for fusing radar and camera data to detect guardrails is presented. An assessment for false positive objects is introduced to verify objects detected by the radar with a vision sensor. In our test methodology a similar approach is applied. Each detected object beside the EVT is assessed as false positive object. The camera image is used for validation. In [18] the authors describe existing approaches to compute a confidence value and introduce a new method to determine a probability of existence using a generalization of Bayes filtering for target tracking. The PoE is clustered in classes ranging from 1 to 7, where 1 represents very unlikely existence and 7 represents a very likely existence of an object. The radar cross section (RCS) value is a quantity to describe obstacles capability to reflect echo signals in direction of the radar receivers. The RCS value of complex shaped targets like vehicles and bikes is dependent on the size, shape, orientation and material, which has influence on tracking stability and target detectability. Therefore, the RCS value of objects is very important for detection, tracking and classification. It can be calculated by

$$\sigma = \frac{(4\pi)^3 R^4}{P_t G^2 \lambda^2} P_r, \tag{10}$$

where σ is the obstacles RCS value, P_t the transmitted power, P_r the received power, R the range from radar to target, G the antenna gain and transmitting wavelength λ [19]. For our test runs each measurement contains following sensor output signals: PoE, RCS, lateral object position relative to the radar sensor and the object ID.

IV. Results

In this section the results of test runs with the EVT for high dynamic and regular driving situations are presented.

A. Evaluation of Probability of Existence

1) High Dynamic Driving Situation: Fig. 5 shows the reference targets mean PoE value as filled circles and all false positive objects PoE generated as squares for 10 test runs during phase I - III. The size of squares represent the quantity of generated objects beside the EVT. In phase I, the mean reference target PoE value has its lowest value at 5.25 and is increasing to 7. Hence, the confidence of the EVT for all measurements reached its maximum. During the first phase no false positive objects were generated. In phase II at t = 0.93 s the mean PoE value of 7 remains for approximately 200 ms. At t = 1.2 s the mean value starts to decrease and reaches its minimum of 3.7 at t = 2.0 s. Depending on the velocity, the test driver starts the intervention between t = 1.5 s... 1.7 s. At t = 1.34 s false positive objects were generated with a PoE value of 3. At t = 1.64 s false positive objects PoE increases to either 6 or 7. The result indicates increased appearance of false positive objects during the high dynamic driving situation. In phase III the PoE of several false positive objects reaches the maximum confidence value in the same cycle. Hence, several objects are detected and forwarded to higher level functions. This can lead to misfiring of irreversible restraint systems.

2) Regular Driving Situation: Fig. 6 shows the mean PoE value and PoE for all false positive objects. The reference targets mean PoE value ranges between 6.9 and 7. The mean PoE value for regular driving situations shows a higher confidence compared to the skid driving situation for approaching a static object. The generated false positive objects are mainly present between t = 0 s and t = 1 s. These objects vary between 2 and 5. Hence, in regular driving situations appear less false positive objects and in case they appear, these objects show lower PoE values compared to high dynamic driving situations.

B. Evaluation of Radar Cross Section

1) Dynamic Driving Situation: Fig. 7 shows the mean reference target RCS value. In phase I the mean reference target RCS value increases to a value of 17 dBsm. No false positive objects were generated. In phase II the mean EVT RCS value reaches a value of 18.8 dBsm at t = 1.3 s. Between t = 1.5 s and t = 1.7 s the mean RCS value remains at similar values for all measurements. At the end of this phase the mean RCS value decreases to 14 dBsm. False positive objects were generated during this phase. Their RCS value varies from 7.5 dBsm to 17.5 dBsm. In phase III the mean RCS value for the EVT ranges around a value of 10 dBsm. An increased number of false positive objects with higher RCS value is present. Hence, the RCS value of the EVT and false positives are similar and can result in false classification.

2) Regular Driving Situation: Fig. 8 shows the RCS values in regular driving situations. The RCS mean value ranges between 15.5 dBsm and 19 dBsm. Compared to the high dynamic driving situation less false positive objects were generated.

Their RCS values range between $9.5\,\mathrm{dBsm}$ and $23.5\,\mathrm{dBsm}$. The false positive objects RCS values in dynamic driving situations are lower compared to regular driving situations.

C. Single Test Run Analysis in Dynamic Driving Situation

Fig. 9 shows the lateral position of detected objects relative to the radar and their PoE over time. Rectangulars, diamonds, crosses and stars represent objects, including false positive ones. They were generated during the skid driving situation. Their size represent the PoE. It is clustered in 3 classes, where class A represents low confidence values, class B medium confidence values and class C high confidence values. The first cycle of measurement is at the start of lateral kick plate movement. The test run is divided into two phases: a clockwise vehicle rotation due to kick plate and a counter clockwise vehicle rotation due to test driver intervention.

1) Clockwise vehicle rotation $0\,\mathrm{s}\ldots2\,\mathrm{s}$*:* The reference target is represented as circles starting at a high PoE. After yaw rate increases to $-30.17\,\mathrm{deg/s}$ the objects lateral position relative to the radar sensor increases according to the vehicle's motion. After some measurement cycles the confidence of the EVT drops to class B and at the same time an additional object with PoE class C is generated. For 11 cycles (approx. $720\,\mathrm{ms}$) during the vehicles rotation two objects with similar PoE differ only by $2\,\mathrm{m}$ lateral position.

2) Counter clockwise vehicle rotation $2\,\mathrm{s}\ldots4\,\mathrm{s}$*:* A similar observation can be seen when the test driver stabilizes the vehicle. Within this time two objects are present with PoE values of class C and class B. Additionally, during the entire skid driving situation several class A objects are generated.

Hence, due to the presence of multiple objects at the same time, whereas in reality only the EVT was present, safety systems (e.g. pre-triggered airbags) could be activated based on false positive objects resulting in fatal consequences for other road users, the own safety and the vehicle.

V. Conclusion and Future Work

This paper introduces a new, non-destructive and reproducible test methodology for automotive surround sensors in high dynamic driving situations. A vehicle motion model describes the dependence between applied lateral force and the vehicle's motion. Real vehicle test runs with an automotive radar sensor measuring a standardized reference target were carried out at a kick plate test track. The kick plate applies a lateral force to the vehicle's rear axle and relevant sensor data were recorded. A set of test runs with the reference target and no lateral force applied at the test vehicle was carried out and compared with the results of high dynamic driving situations. The probability of existence and radar cross section of reference target and generated false positive objects were presented and compared. During a skid driving situation the PoE and RCS values of the reference target decrease, whereas in regular driving situations the values for both remain at a similar value. Furthermore the false positive object generation is increased during the skid driving event. The generated false positive objects show similar features like the present reference target. The sensor limits can be detected by increasing the applied lateral force on the vehicle. The sensor limit is reached when the selection between real object and false positives is impossible, e.g. two objects geometrically close to each other during a skid event. The test vehicle will be upgraded with a reference localization system to assess additional signals.

Acknowledgment

The authors would like to thank Jonas Bielmeier, Raimund Burgmeier, the Federal Ministry of Education and Research (BMBF) and Continental Automotive GmbH for their support.

References

[1] World Health Organization, *Global status report on road safety 2015*. Geneva, Switzerland: World Health Organization, 2015.

[2] Kwanghyun Cho, S. B. Choi, and Hyeongcheol Lee, "Design of an airbag deployment algorithm based on precrash information," *IEEE Transactions on Vehicular Technology*, vol. 60, no. 4, pp. 1438–1452, 2011.

[3] M. Skutek, M. Mekhaiel, and G. Wanielik, "A precrash system based on radar for automotive applications," in *IEEE IV2003 Intelligent Vehicles Symposium. Proceedings*, 9-11 June 2003, pp. 37–41.

[4] R. Moritz, "Pre-crash sensing-functional evolution based on short range radar sensor platform," in *SAE Conference*, 2000.

[5] G. Gstrein, W. Sinz, W. Eberle, Richert J., and Bullinger W., "Improvement of airbag performance through pre-triggering," *Proceedings of the ESV - Enhanced Safety of Vehicles Conference*, 2009.

[6] S. Hasirlioglu, A. Kamann, I. Doric, and T. Brandmeier, "Test methodology for rain influence on automotive surround sensors," in *2016 IEEE Intelligent Transport Systems*, 2016.

[7] Thomas Unger, "Konstellationen bei Auffahrunfällen," *Berichte der ADAC Unfallforschung*, p. 4, 2011.

[8] P. Riekert and T. E. Schunck, "Zur Fahrmechanik des Gummibereiften Kraftfahrzeugs," *Ingenieur-Archiv*, vol. 11, no. 3, pp. 210–224, 1940.

[9] W. Kamm, *Modellversuche und Berechnungen über die Richtungshaltung von Kraftfahrzeugen*. VDI-Verlag, 1963.

[10] D. Schramm, M. Hiller, and R. Bardini, *Vehicle Dynamics: Modeling and Simulation*. Berlin, Heidelberg and s.l.: Springer Berlin Heidelberg, 2014. [Online]. Available: http://dx.doi.org/10.1007/978-3-540-36045-2

[11] H. B. Pacejka, "The wheel shimmy phenomenon: a theoretical and experimental investigation with particular reference to the non-linear problem," Ph.D. dissertation, TU Delft, Delft University of Technology, 1966.

[12] H. B. Pacejka and I. Besselink, *Tire and vehicle dynamics*, 3rd ed. Amsterdam and Boston: Elsevier/BH, 2012. [Online]. Available: http://search.ebscohost.com/login.aspx?direct=true&scope=site&db=nlebk&db=nlabk&AN=453741

[13] Sandner Volker, "Development of a test target for AEB systems," *23rd International Technical Conference on the Enhanced Safety of Vehicles (ESV): Research Collaboration to Benefit Safety of All Road Users*, 2013.

[14] E. Aigner-Breuss, C. Brandstätter, M. Pilgerstorfer, A. Müller, M. Gatscha, "Fahrsicherheitstraining als maßnahme des aktiven risk managements," Wien, 2011.

[15] D. Oprisan and H. Rohling, "Tracking systems for automotive radar networks," in *RADAR 2002*, Oct 2002, pp. 339–343.

[16] M. Benmimoun, A. Pütz, A. Zlocki, and L. Eckstein, *euroFOT: Field Operational Test and Impact Assessment of Advanced Driver Assistance Systems: Final Results*. Berlin, Heidelberg: Springer Berlin Heidelberg, 2013, pp. 537–547.

[17] G. Alessandretti, A. Broggi, and P. Cerri, "Vehicle and guard rail detection using radar and vision data fusion," *IEEE Transactions on Intelligent Transportation Systems*, vol. 8, no. 1, pp. 95–105, March 2007.

[18] R. Altendorfer and S. Matzka, "A new confidence estimator for vehicle tracking based on a generalization of bayes filtering," *IEEE Intelligent Transportation Systems Magazine*, vol. 4, no. 4, pp. 30–41, Winter 2012.

[19] I. Matsunami, R. Nakamura, and A. Kajiwara, "Rcs measurements for vehicles and pedestrian at 26 and 79ghz," in *Signal Processing and Communication Systems (ICSPCS), 2012 6th International Conference on*, 2012, pp. 1–4.

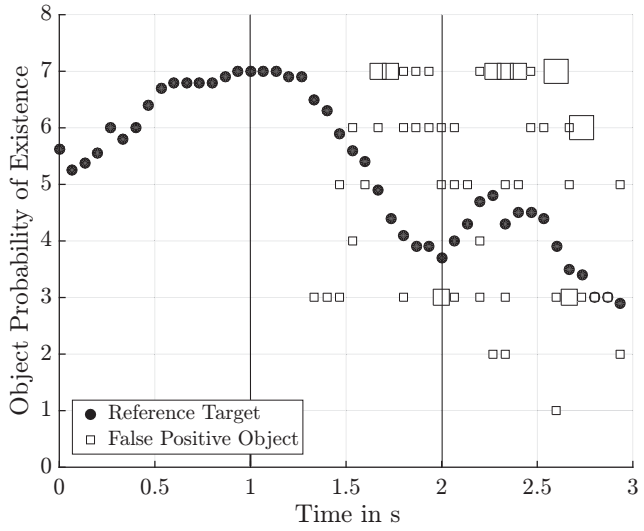

Fig. 5. Object PoE in high dynamic driving situations

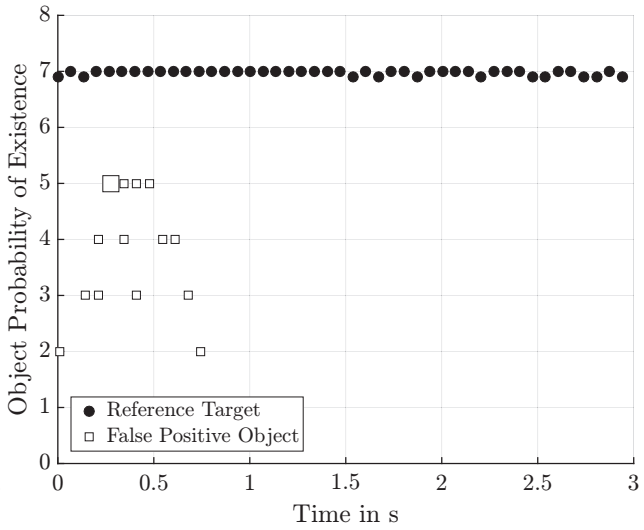

Fig. 6. Object PoE in regular driving situations

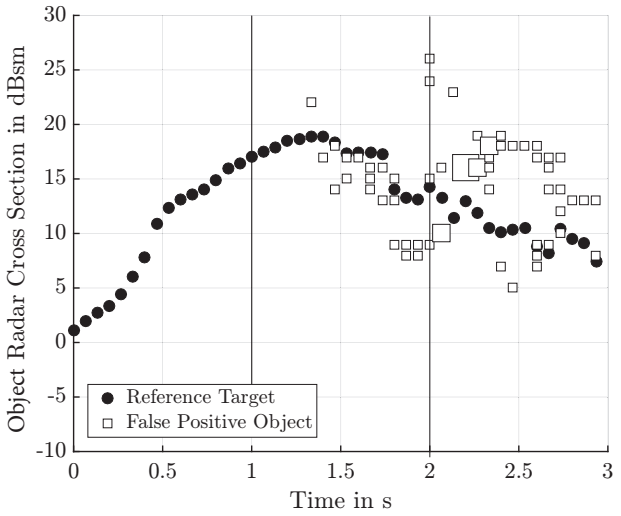

Fig. 7. Object RCS in high dynamic driving situations

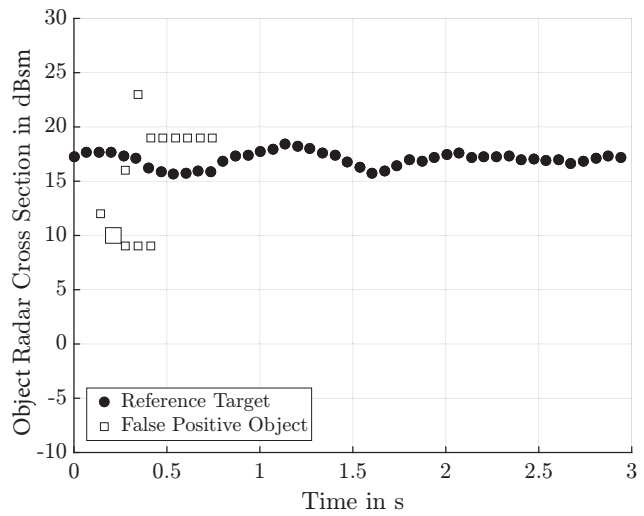

Fig. 8. Object RCS in regular driving situations

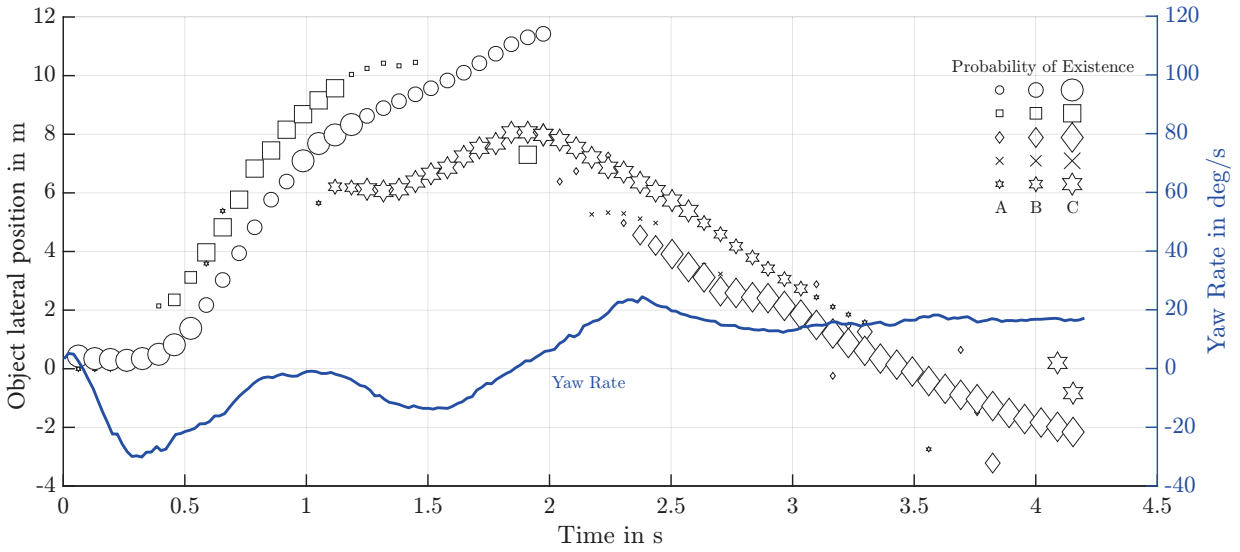

Fig. 9. Object lateral position in high dynamic driving situation